energies

MDPI

Article

Structural and Electrochemical Properties of Dense Yttria-Doped Barium Zirconate Prepared by Solid-State Reactive Sintering

Dae Sik Yun [1,2], Jaegyeom Kim [3], Seung-Joo Kim [3], Jong-Heun Lee [2], Jong-Nam Kim [1], Hyung Chul Yoon [1], Ji Haeng Yu [1], Minseok Kwak [4], Hana Yoon [1], Younghyun Cho [5,*] and Chung-Yul Yoo [1,*]

1 Korea Institute of Energy Research, 152 Gajeong-ro, Yuseong-gu, Daejeon 34129, Korea; daesik1421@gmail.com (D.S.Y.); jnkim@kier.re.kr (J.-N.K.); hyoon@kier.re.kr (H.C.Y.); jhyu@kier.re.kr (J.H.Y.); hanayoon@kier.re.kr (H.Y.)
2 Department of Materials Science and Engineering, Korea University, Seoul 02841, Korea; jongheun@korea.ac.kr
3 Department of Energy Systems Research, Ajou University, Suwon 16499, Korea; jaegyeom86@gmail.com (J.K.); sjookim@ajou.ac.kr (S.-J.K.)
4 Department of Chemistry, Pukyong National University, 45 Yongso-ro, Nam-gu, Busan 48513, Korea; mkwak@pukyong.ac.kr
5 Department of Energy Systems, Soonchunhyang University, Asan 31538, Korea
* Correspondence: yhcho@sch.ac.kr (Y.C.); cyoo@kier.re.kr (C.-Y.Y.); Tel.: +82-41-530-1720 (Y.C.); Fax: +82-41-530-1466 (Y.C.)

Received: 22 October 2018; Accepted: 5 November 2018; Published: 8 November 2018

Abstract: For practical utilization of proton-conducting ceramic fuel cells and electrolyzers, it is essential to lower the sintering temperature and processing time of $BaZrO_3$-based proton conductors. We investigated the effect of sintering temperature and time on the structural and electrochemical properties of dense $BaZr_{0.8}Y_{0.2}O_{3-\delta}$ (BZY) prepared by a solid-state reactive sintering process, using NiO as a sintering aid. The sintered BZY prepared from the micronized precursor powder exhibited a density higher than 93%, and an average grain size in the range of 0.6 to 1.4 μm. The orthorhombic BaY_2NiO_5 phase was also observed in the sintered BZY from the combined conventional and synchrotron X-ray diffraction measurements. Electrochemical impedance spectroscopy showed that the total proton conductivities of BZY can be modulated by sintering temperature in a wet reducing atmosphere. The maximum total ion transport number achieved was 0.89 at 600 °C, and the maximum power density of the symmetric BZY electrolyte supported cell with Pt electrodes was 5.24 $mW \cdot cm^{-2}$ at 900 °C.

Keywords: proton-conducting oxides; $BaZrO_3$; electrochemical properties; solid-state reactive sintering

1. Introduction

Y-doped $BaZrO_3$ ($BaZr_{1-x}Y_xO_{3-\delta}$) is a suitable material for use as an electrolyte in proton-conducting ceramic fuel cells (PCFCs) and electrolyzers, because of its excellent chemical stability and adequate proton conductivity [1–3]. The main advantages of PCFCs over conventional solid oxide fuel cell using (O^{2-} conducting electrolyte) are the lack of dilution of fuel by the generated steam and a low operating temperature (below 600 °C). However, to realize dense $BaZr_{1-x}Y_xO_{3-\delta}$ requires a high sintering temperature (≥1600 °C) and long sintering time (≥24 h) [4–7], which limits the practical utilization for PCFCs. Furthermore, it results in the volatilization of the barium component

during the high-temperature sintering process, and consequent precipitation of a secondary phase, such as Y_2O_3 [8,9], which significantly reduces the proton conductivity of the $BaZr_{1-x}Y_xO_{3-\delta}$ electrolyte [4].

Therefore, for the development of practical PCFCs, increasing effort has been applied to lowering the temperature and time for $BaZr_{1-x}Y_xO_{3-\delta}$ sintering. Recently, various transition metal oxides have been explored as sintering aids to decrease the sintering temperature and time [6,10–16]. Babilo and Haile [6] demonstrated that adding small amounts of transition metal oxides to $BaZr_{1-x}Y_xO_{3-\delta}$ powder significantly enhanced the densification of $BaZr_{1-x}Y_xO_{3-\delta}$. Tong et al. [17–19] suggested a solid-state reactive sintering (SSRS) process to produce refractory proton-conducting oxides by combining solid-state synthesis and reactive sintering processes. In the SSRS process, the addition of only a small amount of a sintering aid was sufficient to achieve proton-conducting oxides in a desired crystalline phase. In addition, the further densification/grain growth of the synthesized phase to a fully dense specimen could be realized through a single-step process. NiO is one of the ideal sintering agents to reduce $BaZr_{0.8}Y_{0.2}O_{3-\delta}$ sintering temperature and processing time in the SSRS [19]. The addition of 2 wt.% NiO as a sintering aid did not reduce the proton conductivity of $BaZr_{0.8}Y_{0.2}O_{3-\delta}$ electrolytes prepared by the conventional solid-state reaction [20]; however, the detrimental effect of NiO sintering aid on the transport properties of $BaZr_{1-x}Y_xO_{3-\delta}$ is also reported in the literature [21,22]. Although there have been reports on the preparation, conductivity, and mechanical behavior of dense $BaZr_{1-x}Y_xO_{3-\delta}$ sintered using NiO sintering aids [17–19,23,24], systematic investigation of the structural and electrochemical properties of dense $BaZr_{0.8}Y_{0.2}O_{3-\delta}$ prepared by means of SSRS with a NiO sintering aid is still needed. In the present study, we investigate the effect of sintering conditions, including sintering time and temperature during SSRS, on various properties, such as the crystal/micro structure, total/grain/grain boundary conductivity, electromotive force, and fuel cell performance. To the best of our knowledge, this is the first systematic study on the structural and electrochemical properties of dense $BaZr_{0.8}Y_{0.2}O_{3-\delta}$ prepared by SSRS, with 2 wt.% NiO used as a sintering aid.

2. Experimental

2.1. Preparation of Dense $BaZr_{0.8}Y_{0.2}O_{3-\delta}$

Dense $BaZr_{0.8}Y_{0.2}O_{3-\delta}$ (BZY) pellets were prepared by solid-state reactive sintering (SSRS). Stoichiometric amounts of $BaCO_3$ (≥99%, Sigma-Aldrich), ZrO_2 (99%, Junsei, Chuo-ku, Tokyo), and Y_2O_3 (99.99%, Sigma-Aldrich, St. Louis, MI, USA) with 2 wt.% NiO (99.99%, Sigma-Aldrich) as a sintering aid were ball-milled at 120 rpm in ethanol for 24 h with zirconia balls. The ball-milled powder was dried at 70 °C using a rotary evaporator (OSB-2000, Eyela, New York, NY, USA). To investigate the effect of particle size, the precursor powder was pulverized further using a planetary ball mill (Pulverisette 6, Fritsch, Idar-Oberstein, Germany) at 300 rpm for 5 h. The weight proportions of the precursor powder, ethanol, and zirconia ball mixture (three-ball mixture with diameters of 1, 3, and 10 mm) were 1:2:5. The particle size of the precursor powder was analyzed using a particle size analyzer (La-950 V2, Horiba, Fukuoka, Japan). The powder was uniaxially pressed into green pellets 25.4 mm in diameter under a pressure of 25 MPa for 1 min. The pellets were covered with calcined $BaZr_{0.8}Y_{0.2}O_{3-\delta}$ powder to prevent volatilization of the barium, and sintered at temperatures ranging from 1435 to 1535 °C at 50 °C intervals for (5–25) h in ambient air. The relative density of the BZY pellets was measured in ethanol media using Archimedes' method. The phases and lattice parameters of the sintered pellets were characterized using X-ray diffraction (XRD, Rigaku 2200, Tokyo, Japan). The XRD patterns were obtained at room temperature in the 2θ range from 20 to 80°, and the corresponding lattice parameters were calculated using the FullProf program [25]. Synchrotron X-ray diffraction measurements were conducted using the high-resolution powder diffraction at the 9B beamline of the Pohang Light Source (Pohang Accelerator Laboratory, Korea). A crushed BZY powder sample was exposed to a monochromatic 1.5184 Å X-ray beam, and the diffraction pattern was measured in the 2θ range from 10–130° at intervals of 0.01°. The data obtained were analyzed using the

FullProf program [25]. The microstructure of the sintered pellets was investigated by scanning electron microscopy (SEM, S-4700, Hitachi, Tokyo, Japan). The chemical composition of the BZY pellets sintered for 15 h was measured using inductively coupled plasma optical emission spectroscopy (ICP-OES, ICP-OES 720, Agilent, Santa Clara, CA, USA).

2.2. Measurement of Electrochemical Properties of the Dense $BaZr_{0.8}Y_{0.2}O_{3-\delta}$

The BZY pellets were polished to a thickness of 1 mm using SiC sandpaper ((100–1200) grit), brush-coated on both sides using a Pt paste (6926, Heraeus, Hanau, Germany), and treated at 900 °C for 1 h to investigate their electrochemical properties. Electrochemical impedance spectroscopy (EIS, Metrohm, Autolab, Utrecht, Netherland) measurements were performed at temperatures of 100 to 600 °C at 50 °C intervals under a humidified reducing atmosphere (3% H_2 balanced in Ar, $p(H_2O)$ = 0.03 atm) in the frequency range of 1 MHz to 0.1 Hz. The EIS spectra were fitted and analyzed using Z-view software (Scribner Associates Inc., Southern Pines, NC, USA). To investigate the electromotive force (EMF) and current–voltage behavior, BZY discs were sealed onto an alumina reactor using a gold ring, and heated at 1050 °C for 1 h. Humidified air ($p(H_2O)$ = 0.03 atm) and H_2 ($p(H_2O)$ = 0.03 atm) gas were supplied to the cathode and anode, respectively. EMF values and current–voltage curves were measured in the temperature range of 600 to 900 °C.

3. Results and Discussion

3.1. Sintering Behavior and Structure of $BaZr_{0.8}Y_{0.2}O_{3-\delta}$

Figure 1a shows a photograph of the sintered $BaZr_{0.8}Y_{0.2}O_{3-\delta}$ (BZY) pellets produced from the precursor ($BaCO_3$, ZrO_2, Y_2O_3, and NiO) mixtures with only conventional ball milling (left in Figure 1a), and with an additional planetary ball milling (right in Figure 1a). The BZY pellets produced from the conventional, only ball-milled precursor powder exhibited apparent bending and cracks after sintering. In contrast, when planetary ball milling was additionally employed after the conventional ball milling process, crack-free BZY pellets were obtained. Dilatometry experiments have shown that during SSRS, abrupt expansion of green BZY pellets followed by sintering shrinkage occurs, because of the release of CO_2 from the precursor powder [26], which can cause cracking and bending of BZY pellets. Additional planetary ball milling to micronize the precursor powders prevents the crack formation and bending of BZY pellets during SSRS, as shown in Figure 1a. Figure 1b the particle size distribution of the precursor powders produced with and without additional planetary ball milling. The particle sizes of the ball-milled precursor powder are in the range of 0.2–10 μm, while that with additional planetary ball milling ranges from 0.2 to 4 μm. After an additional planetary ball milling, the median particle size decreased from 3.0 to 1.1 μm. At the same time, the size distribution also decreased. Thus, it was confirmed that a smaller median particle size and narrower particle distribution of the precursor powder was beneficial in obtaining dense, crack-free BZY pellets by the SSRS method. Furthermore, when an additional planetary ball milling was performed, regardless of the sintering temperature and time, denser BZY pellets with a density higher than 94% were obtained. On the other hand, dense BZY pellets could only be obtained with the ball-milled precursor powder at high sintering temperature and long sintering time (1535 °C and 15 h, respectively). Table 1 summarizes the densities of the BZY pellets sintered by the SSRS process. For the comparison, we also sintered BZY using the planetary ball-milled $BaCO_3$, ZrO_2, and Y_2O_3 powder, without the NiO sintering aid. The density of BZY sintered at 1485 °C for 15 h was only 58%, which confirms that the NiO (2 wt.%) plays an important role in realizing high density BZY pellets.

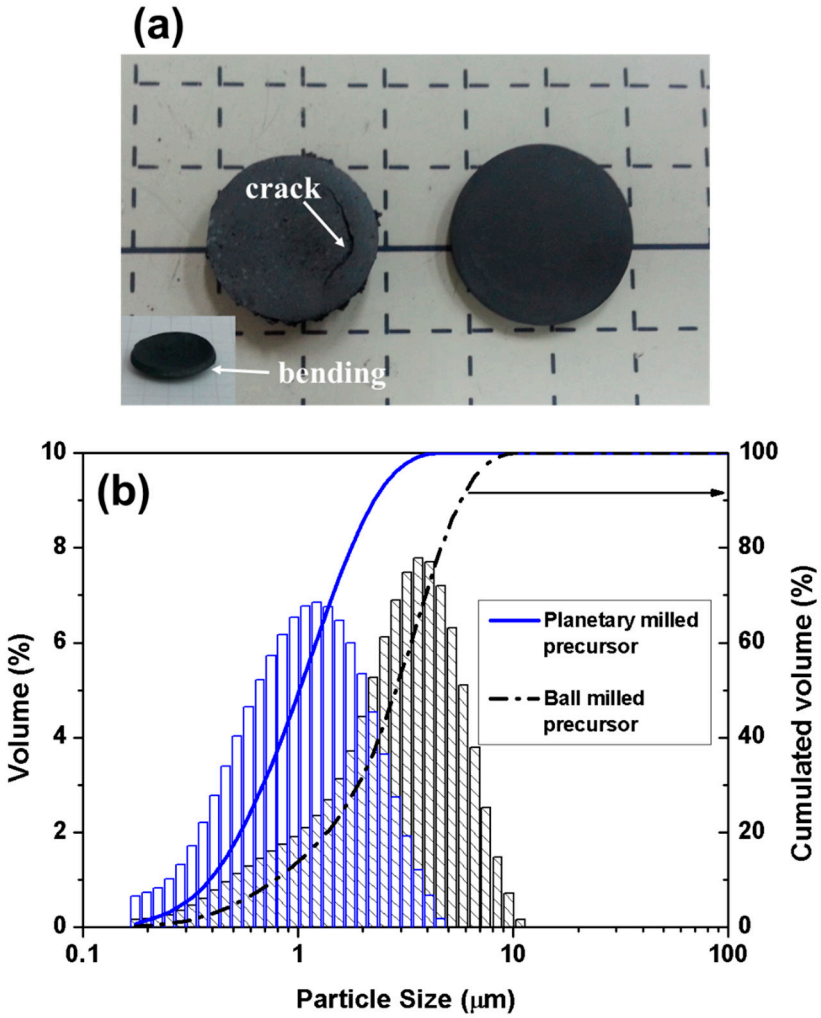

Figure 1. (**a**) Photograph of $BaZr_{0.8}Y_{0.2}O_{3-\delta}$ (BZY) pellets sintered at 1485 °C for 15 h, using ball-milled (left) and planetary ball-milled precursor powders (right); and (**b**) particle size distributions of ball-milled and planetary ball-milled precursor powders.

Table 1. Relative densities of sintered $BaZr_{0.8}Y_{0.2}O_{3-\delta}$ (BZY) pellets prepared using ball-milled (left) and planetary ball-milled precursor powders (right) at different sintering times and temperatures.

Relative Density (%)		Ball-Milled Precursor			Planetary Ball-Milled Precursor		
		Temperature (°C)			Temperature (°C)		
		1435	1485	1535	1435	1485	1535
Time (h)	5	56	-	87	94	94	94
	10	-	82	-	-	94	-
	15	70	-	94	94	95	95
	20	-	-	-	-	95	-
	25	-	-	-	-	95	-

In order to confirm the effect of sintering conditions during SSRS on the microstructures and phases of BZY, we modulated the sintering time and temperature. Figure 2 shows the SEM images of sintered BZY pellets produced with and without the additional planetary ball milling process at various sintering times and temperatures. The grain size gradually increased with higher sintering time and temperature for both cases (Table 2). However, the average grain size of the BZY pellets obtained using the planetary ball-milled precursor powder was in the range of 0.61–1.39 μm, while that of the BZY pellets obtained using the ball-milled precursor powder was in the range of 0.51–1.19 μm,

as estimated from the SEM image. Furthermore, the BZY sintered at 1435 °C for 5 and 15 h. utilizing only conventional ball milling (Figure 2a,c), do not fully form a flat surface at micrometer scale. The SEM images and measured density of the BZY confirmed that the sintered BZY produced using the larger powder produced by only ball-milled precursor (without planetary ball milling) had a lower density than that produced from the larger powder generated by planetary ball milling. Figure 3 shows the SEM images of the sintered BZY as a function of the sintering time at 1485 °C for the planetary ball-milled precursor powder. This figure shows that with increasing sintering time from 5 to 25 h, the grain size of BZY increased from 0.83 to 1.16 μm. Such results agreed with the grain growth behaviors that are typically observed.

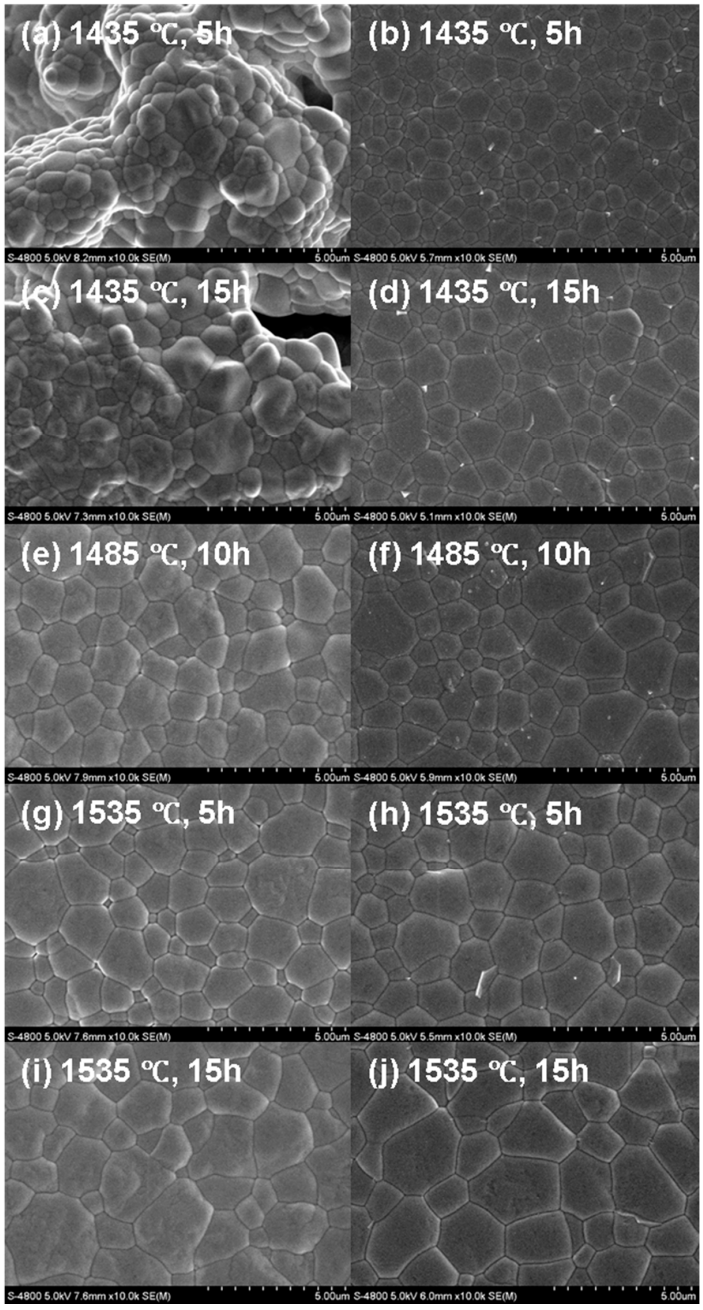

Figure 2. SEM images of BZY pellets sintered at different sintering temperature and for different times, using ball-milled (**left**) and planetary ball-milled precursor powders (**right**).

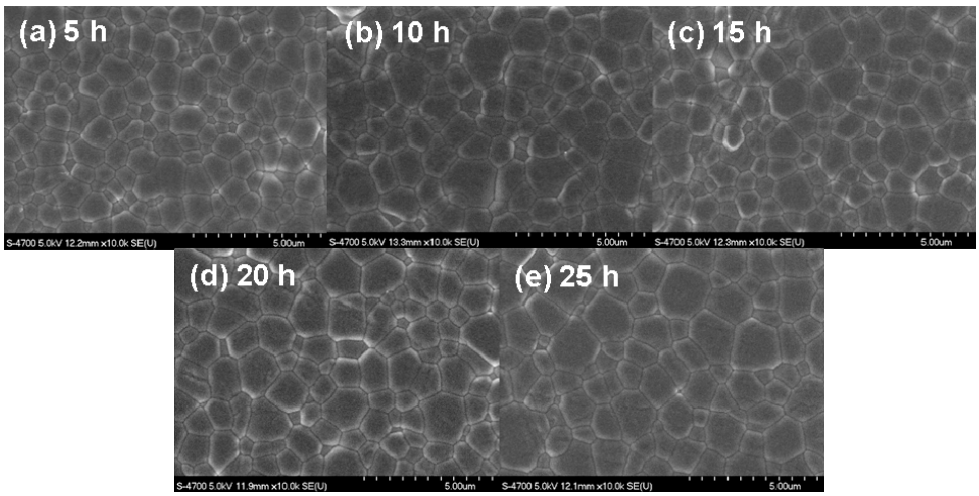

Figure 3. SEM images of BZY pellets sintered using the planetary ball-milled precursor powder at 1485 °C, for (**a**) 5, (**b**) 10, (**c**) 15, (**d**) 20, and (**e**) 25 h.

Table 2. Average grain size of sintered BZY pellets prepared using ball-milled (left) and planetary ball-milled precursor powders (right) at different sintering times and temperatures.

Grain Size (μm)		Ball-Milled Precursor			Planetary Ball-Milled Precursor		
		Temperature (°C)			Temperature (°C)		
		1435	**1485**	**1535**	**1435**	**1485**	**1535**
Time (h)	5	0.51	-	1.02	0.61	0.83	1.06
	10	-	0.88	-	-	0.93	-
	15	0.72	-	1.19	0.82	0.96	1.39
	20	-	-	-	-	1.04	-
	25	-	-	-	-	1.16	-

Figure 4a shows the XRD patterns of the BZY samples prepared by sintering of planetary ball-milled precursor powders at 1435, 1485, and 1535 °C for 15 h, respectively. In the BZY sample sintered at 1435 °C for 15 h, cubic BZY perovskite (space group $Pm\bar{3}m$) and unreacted cubic Y_2O_3 (space group $Ia\bar{3}$) phases were observed, whereas the BZY samples sintered at 1485 and 1535 °C for 15 h showed cubic BZY with orthorhombic BaY_2NiO_5 (space group *Immm*) phases, and the unreacted cubic Y_2O_3 peak mostly disappears. Such changes in the Y_2O_3 secondary phase at the different sintering temperatures suggests that it is necessary to perform SSRS at temperatures higher than 1485 °C. To study the effect of the sintering time on the phase formation, BZY samples prepared from the planetary ball-milled precursor powder were sintered at 1485 °C for (5 to 25) h at 5 h intervals. The XRD patterns (Figure 4b) confirm that the sintering time does not significantly affect the crystalline phases of the sintered BZY. The lattice parameter was approximately 4.21 Å for all of the sintered BZY samples regardless of sintering time, which is in a good agreement with the values reported in the literature [17–20,23,24]. The lattice parameter of BZY given in Table 3 decreased with Ba deficiency and/or Y_2O_3 secondary phase formation [27]; hence, it can be seen that 15 h is the minimum sintering time for obtaining dense BZY by means of SSRS with least variation in the nominal BZY composition. In addition, the actual chemical compositions of sintered BZY for 15 h were determined by ICP-OES. The compositions of BZY sintered at 1435 and 1485 °C are $Ba_{0.99}Zr_{0.79}Y_{0.22}O_{3-\delta}-0.044BaY_2NiO_5$ and $Ba_{0.98}Zr_{0.80}Y_{0.22}O_{3-\delta}-0.043BaY_2NiO_5$, respectively, while that of BZY sintered at 1535 °C is $Ba_{0.93}Zr_{0.82}Y_{0.23}O_{3-\delta}-0.046BaY_2NiO_5$, under the assumption that Ni is present in the compound of BaY_2NiO_5. The significant evaporation of Ba is observed for the BZY sintered at 1535 °C. Combined XRD and ICP-OES results suggest that dense BZY pellets could be prepared at the optimized sintering condition of BZY at 1485 °C for 15 h.

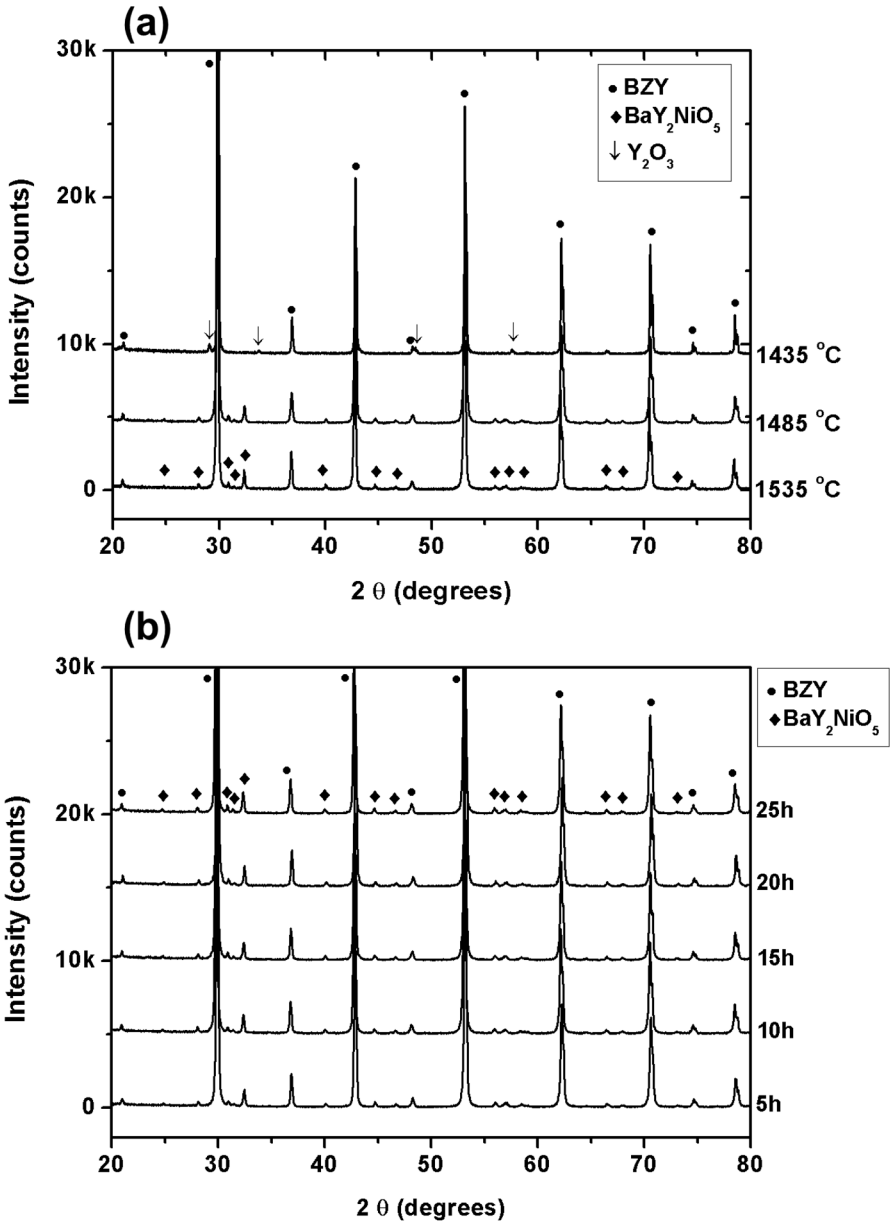

Figure 4. (**a**) XRD patterns of BZY pellets sintered using the planetary ball-milled precursor powder at different sintering temperature of 1435, 1485, and 1535 °C for 15 h, and (**b**) XRD patterns of BZY pellets sintered using the planetary ball-milled precursor powder at 1485 °C for different sintering times of 5, 10, 15, 20, and 25 h.

Table 3. Lattice parameters of sintered BZY pellets prepared using planetary ball-milled precursor powders at different sintering times and temperature.

Lattice Parameter (Å)		Planetary Ball-Milled Precursor		
		Temperature (°C)		
		1435	1485	1535
Time (h)	5	4.213	4.211	4.208
	10	-	4.211	-
	15	4.211	4.212	4.213
	20	-	4.209	-
	25	-	4.206	-

Azad et al. [28] have reported that two cubic phases are observed for 10 mol.% $BaZr_{1-x}Y_xO_{3-\delta}$, due to the cross substitution of Y from B-sites onto the A-sites. In order to investigate the crystal structure in detail, a synchrotron X-ray diffraction pattern was obtained for the crushed powder from sintered BZY (1485 °C for 15 h). Figure 5 shows the observed, calculated, and difference profiles of the synchrotron X-ray diffraction pattern. Table 4 summarizes the structural parameters and residual indices from the Rietveld refinement. The refinement results confirm that all of the diffraction peaks are consistent with single-phase cubic BZY and orthorhombic BaY_2NiO_5 as a minor impurity phase. The calculated weight fractions of BZY and BaY_2NiO_5 from the final Rietveld refinement run were 94 and 6%, respectively.

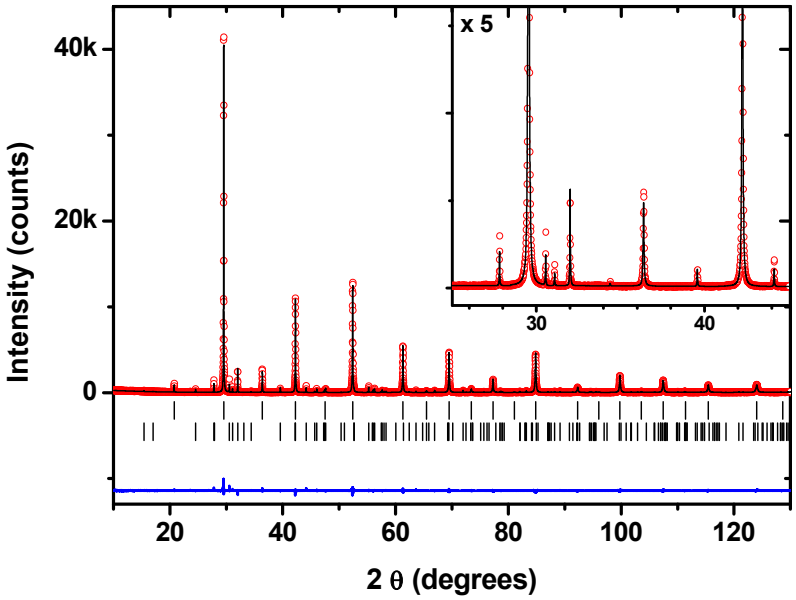

Figure 5. Synchrotron X-ray powder diffraction pattern for the crushed powder of the BZY pellet sintered at 1485 °C for 15 h. The observed data are represented by circles, and the solid lines are the result of Rietveld refinements for the cubic BZY and orthorhombic BaY_2NiO_5. The difference profile is also shown (lower line). Tick marks indicate the Bragg positions of BZY (**upper**) and BaY_2NiO_5 (**lower**).

Table 4. Structural parameters and residual indices determined from synchrotron XRD data for $BaZr_{0.8}Y_{0.2}O_{3-\delta}$ and BaY_2NiO_5.

(a) $BaZr_{0.8}Y_{0.2}O_{3-\delta}$, space group: $Pm\bar{3}m$, a = 4.21163 (1) Å					
Atom	**Site**	**x**	**y**	**z**	**U_{iso} (100 * Å^2)**
Ba	1*b*	0.5	0.5	0.5	1.30 (1)
Zr/Y	1*a*	0.0	0.0	0.0	0.46 (1)
O1	3*d*	0.5	0.0	0.0	1.80 (5)
(b) BaY_2NiO_5, space group: *Immm*, a = 3.76162 (1) Å, b = 5.76193 (2) Å, c = 11.33135 (5) Å					
Atom	**Site**	**x**	**y**	**z**	**U_{iso} (100 * Å^2)**
Ba	2*a*	0.5	0.5	0.0	1.1 (1)
Ni	4*j*	0.0	0.0	0.0	1.9 (2)
Y	2*c*	0.5	0.5	0.2018 (3)	0.75 (9)
O1	2*d*	0.0	0.211 (3)	0.152 (1)	1.1 (3)
O2	8*l*	0.5	0.0	0.0	1.1 (3)

R_p = 7.37%, R_{wp} = 10.7%, R_{exp} = 8.24%, χ^2 = 1.67.

3.2. Electrochemical Properties of $BaZr_{0.8}Y_{0.2}O_{3-\delta}$

To evaluate the electrochemical properties of dense BZY samples sintered at 1435, 1485, and 1535 °C for 15 h, EIS measurements were conducted in the temperature range 100 to 600 °C. Even though oxygen ions, protons, and holes are potential charge carriers in $BaZrO_3$-based proton-conducting oxide, at temperatures below 600 °C under a reducing atmosphere, the protons play a major role in the charge carrier, because the diffusion coefficient of protons is much higher than those of holes and oxygen ions [29]. Therefore, in the present study, proton conductivity was measured under a reducing wet atmosphere (3% H_2 in Ar and pH_2O = 0.03 atm). Cole–Cole plots are typically used to determine the grain (R_b and CPE_b), grain boundary (R_{gb} and CPE_{gb}), and electrode (R_{elec} and CPE_{elec}) contributions [6–8,13,30,31]. Figure 6 shows the Cole–Cole plots obtained for the sintered BZY samples. Figure 6a shows that the grain arc could not be clearly distinguished in the temperature range of 400 to 600 °C, because of the frequency limit (1 MHz) of the impedance analyzer. Therefore, only the grain resistance was obtained from the real axis intercept at high frequency. In contrast, the grain arc was observed below 200 °C, as shown in Figure 6b, which enables the grain capacitance to be determined. Figure 6 also includes equivalent circuit fitting. In the equivalent circuit, a constant-phase element (CPE) was used for fitting of the depressed arc described by $\text{CPE} = \left[Y_0(jw)^n\right]^{-1}$, where w is the frequency, Y_0 is the non-Debye capacitance, and n is the phase-angle parameter of the constant-phase element. The capacitance of each arc contribution can be calculated using $C = \frac{(R_0Y_0)^{\frac{1}{n}}}{R_0}$, where R_0 is the resistance parallel to CPE. Figure 7a plots the total proton conductivity of the BZY samples as a function of the inverse of the temperature. Among the BZY samples, the BZY sample sintered at 1435 °C exhibited a rather low conductivity compared to the other samples, throughout the entire temperature range. At 500 °C, total conductivity values of ((2.28, 1.15, and 2.01) $\times$ 10^{-3}) S·cm^{-1} were obtained for the sample sintered at 1485, 1435, and 1535 °C, respectively. The activation energies of the samples sintered at 1435, 1485, and 1535°C were 0.51, 0.52, and 0.44 eV, respectively, in the temperature range of 100 to 500 °C. The total conductivity of all of the BZY samples exhibited a change in slope at approximately 550 °C, because of the decrease in the concentration of protons in the BZY lattice [17,20]. The conductivity and activation energy values obtained in this study are consistent with the conductivity reported in the literature for BZY prepared by SSRS with a 1 wt.% NiO sintering aid (1.6 $\times$ 10^{-3} S·cm^{-1}) [13]. Therefore, it could be concluded that the relatively high amount of NiO sintering aid used in this study had little impact on the total proton conductivity of the BZY in the temperature range (300 to 500) °C, except for the BZY sintered at 1435 °C. This suggests that the unincorporated Y_2O_3 phase plays a detrimental role in proton conduction, as indicated in the X-ray diffraction patterns (Figure 4a), since the unincorporated Y_2O_3 results in the decrease of proton concentration of BZY. The conductivity values measured at temperature below 200 °C were much lower compared with those measured at a temperature higher than 200 °C (by a factor of ~5 to 12), which suggests that the effect of secondary and impurity phases (BaY_2NiO_5 and Y_2O_3) is apparent at temperatures below 200 °C. Table 5 summarizes the conductivities obtained in this study, and those reported in the literature for BZY at temperatures between 500 and 600 °C under wet inert and reducing atmospheres. The comparison of total proton conductivities in this study and the literature indicates that 2 wt.% NiO sintering aid is not significantly detrimental for proton conduction in the BZY electrolyte.

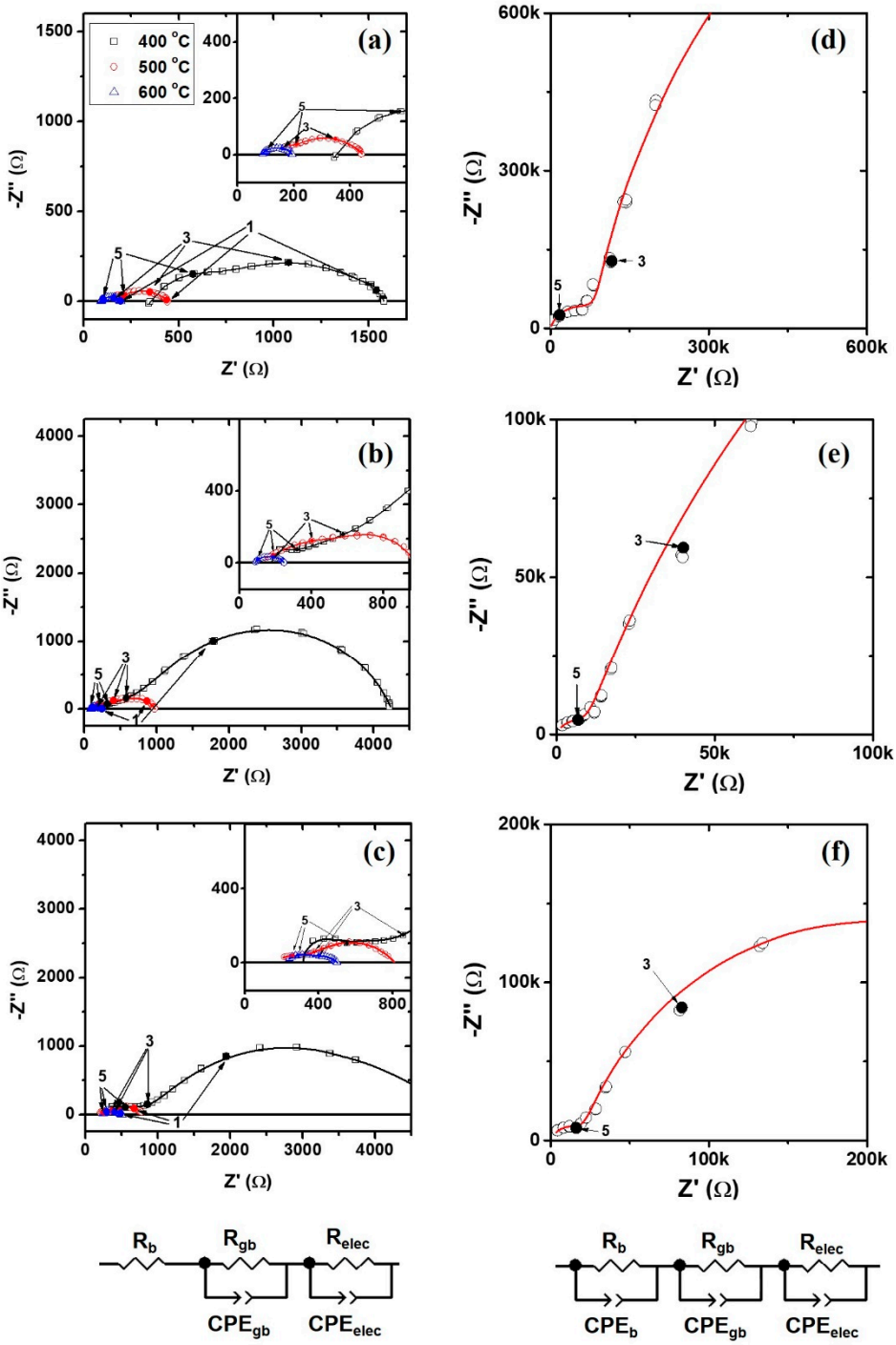

Figure 6. Nyquist plots of BZY sintered at different temperature of (**a**,**d**) 1435 °C, (**b**,**e**) 1485 °C, and (**c**,**f**) 1535 °C for 15 h at 400–600 °C (**left**) and 100 °C (**right**) in wet 3% H_2 balanced in Ar ($p(H_2O)$ = 0.03 atm). The solid line is the fitting data for an equivalent electrical circuit (inset). The numbers used to label the spectra denote the logarithmic values of the frequency (Hz).

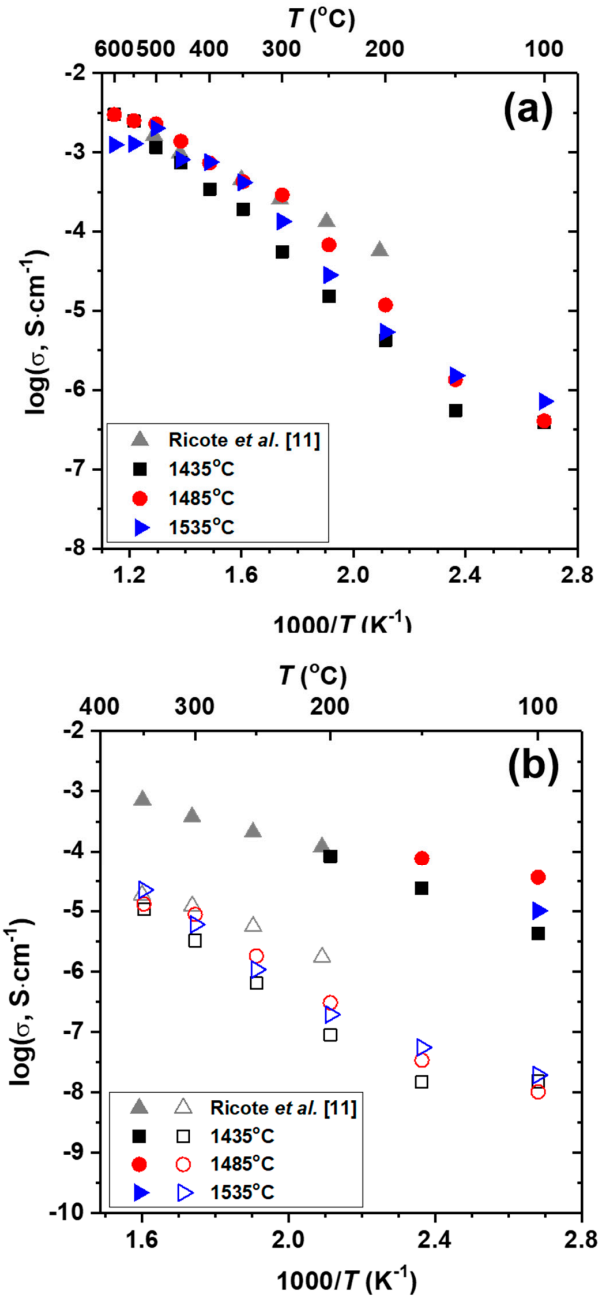

Figure 7. (**a**) Total proton conductivity, and (**b**) bulk (filled symbols) and specific grain-boundary (empty symbols) conductivities of BZY sintered at different temperatures of 1435, 1485, and 1535 °C for 15 h as a function of the inverse temperature under wet 3% H_2 balanced in Ar ($p(H_2O)$ = 0.03 atm).

Table 5. Proton conductivity of $BaZr_{0.8}Y_{0.2}O_{3-\delta}$ at 500 and 60) °C under wet reducing atmosphere, in this study and in the literature.

$BaZr_{0.8}Y_{0.2}O_{3-\delta}$ Powder Synthesis Method	Sintering T and Time (°C/h)	Conductivity (mS·cm^{-1}, 600 °C)	Conductivity (mS·cm^{-1}, 500 °C)	Atmosphere (gas/atm with H_2O)	Reference
Glycine-nitrate combustion	1600/10	6.91	5.2	N_2/0.03	[4]
Sol-gel combustion	1500/6	2.14	1.12	Ar/0.03	[8]
Sol-gel combustion	1600/6	4.45	2.95	Ar/0.03	[10]
Solid-state reactive sintering	1500/24	33.1	16.9	Ar/0.03	[15]
Solid-state reaction	1450/5	3.09	1.26	Ar/0.03	[18]
Solid-state reaction	1675/10	3.62	2.03	40% H_2/0.04	[27]
EDTA-citric acid precipitation	1600/24	22.9	14.8	N_2,/0.03	[29]
Solid-state reactive sintering	1435/15	3.00	1.15	3% H_2/0.03	This study
Solid-state reactive sintering	1485/15	3.00	2.28	3% H_2/0.03	This study
Solid-state reactive sintering	1535/15	1.24	2.01	3% H_2/0.03	This study

The brick layer model is typically used to describe the physical properties of polycrystalline materials. The specific grain boundary conductivity is given by $\sigma_{sp.gb} = \frac{1}{R_{gb}} \frac{L}{A} \frac{C_{bulk}}{C_{gb}}$, where R_{gb} is the grain boundary resistance, C_{gb} is the grain boundary capacitance, C_{bulk} is the bulk capacitance, L is the sample thickness, and A is the electrode area. When the grain boundary capacitance cannot be extracted from the impedance spectra, the specific boundary conductivity is calculated using $\sigma_{sp.gb} = \frac{1}{R_{gb}} \frac{L}{A} \frac{\delta}{D}$, under the assumption that the grain boundary thickness and grain size remain effectively constant. Here, δ is the grain boundary thickness, and D is the grain size. Figure 7b shows the grain conductivity and specific grain boundary conductivity of the samples as a function of the inverse of temperature. The conductivity data reported in the literature [13] for BZY prepared by SSRS with a 1 wt.% NiO sintering aid are included for comparison. The grain conductivity was much higher than the grain boundary conductivity, which is consistent with the results reported in the literature for $BaZrO_3$-based proton-conducting oxides. The specific grain boundary conductivity obtained in this study was significantly lower than that reported for BZY prepared by SSRS with a 1 wt.% NiO sintering aid [13] below 350 °C, whereas the grain conductivity was comparable. The significantly lower grain boundary conductivity obtained in this study might be due to the higher amount of the BaY_2NiO_5 secondary phase, resulting from the relatively high amount of the NiO sintering aid (2 wt.% NiO). This is consistent with the finding reported in the literature that the secondary phase is mainly segregated at the grain boundary by introducing a sintering aid [32]. The activation energy values of the grain and specific grain boundary conductivities were in the ranges 0.33–0.39 and 0.35–0.45 eV, respectively, which is consistent with the values of 0.39 and 0.45 eV, respectively, reported in the literature for BZY prepared using SSRS [13].

Table 6 shows the bulk dielectric constant (ε_r), Debye length (λ), and Mott–Schottky depletion length (λ*) of BZY at 100 °C, calculated using $\varepsilon_r = \frac{C_{bulk} L}{\varepsilon^0 A}$, $\lambda = \sqrt{\frac{kT\varepsilon_r\varepsilon^0}{2e^2 C_H}}$, and $\lambda^* = 2\lambda\sqrt{\frac{e\Delta\phi(0)}{kT}}$, respectively. In these equations, C_H is the proton concentration of BZY (2.50×10^{26} m^{-3}) estimated in the literature [20]; $\Delta\phi(0)$ is the barrier height at the center of the grain boundary, determined from $\frac{\sigma_{bulk}}{\sigma_{GB}} = \frac{e^{\frac{e\Delta\phi(0)}{kT}}}{2\frac{e\Delta\phi(0)}{kT}}$; ε^0 is the vacuum permittivity. A is the area of the sample; L is the thickness of the sample; k is the Boltzmann's constant; and e is the electron charge. It is generally believed that the arc in the high-frequency region exhibits a value for the proton-conducting oxide grain (C = ~10^{-11} F), and that the arc in the intermediate-frequency region exhibits a value for the grain boundary (C = ~10^{-9} F) [6–8,13,30,31] that is in agreement with this study. The bulk dielectric constants of BZY obtained in this study were higher than those (37–155) reported in the literature [13,31,33,34]. However, the Debye length, Mott–Schottky depletion length, and barrier height values obtained in this study were fairly consistent with the ranges of values of 0.26–0.35 nm, 0.5–1.4 nm, and 0.04–0.35 V, respectively) reported for BZY in the literature [13,33,34].

Table 6. Bulk pseudocapacitance (C_{bulk}), grain-boundary pseudocapacitance (C_{GB}), dielectric constant (ε_r), Debye length (λ), barrier height at the grain boundary core ($\Delta\phi(0)$), and Mott–Schottky depletion width (λ*) of BZY at 100 °C under wet 3% H_2 balanced in Ar ($p(H_2O)$ = 0.03 atm).

Sintering Temperature (°C)	**1435**	**1485**	**1535**
Sintering Time (h)	**15**	**15**	**15**
C_{bulk} (F)	6.64×10^{-11}	9.60×10^{-11}	6.64×10^{-11}
C_{GB} (F)	1.88×10^{-9}	3.88×10^{-9}	1.88×10^{-9}
ε_r	266	384	266
λ (nm)	0.35	0.42	0.60
$\Delta\phi(0)$	0.18	0.29	0.09
λ* (nm)	1.47	2.22	1.02

3.3. Electromotive Force Characteristics and Fuel Cell Performance

The performance and characteristics of the BZY sample sintered at 1485 °C for 15 h, which exhibited the best conductivity, were investigated by means of electromotive force (EMF) and current–voltage measurements. The theoretical value of the EMF was calculated using $EMF_{theoretical} = E_0 + \frac{RT}{2F} \ln\left(\frac{P_{O_2}^{0.5} P_{H_2}}{P_{H_2O}}\right)$, where $E_0 = \frac{\Delta G_0}{2F}$, ΔG is the Gibbs free energy for standard conditions, and P_{O_2}, P_{H_2}, and P_{H_2O} are the partial pressures of oxygen, hydrogen, and water, respectively. Figure 8a presents the measured and theoretical EMF values, together with the ion transport number ($EMF_{measured}/EMF_{theoretical}$). The ion transport number was found to decrease with increasing temperature from 0.89 to 0.7) at(600 to 900 °C, because of the decrease in the proton concentration in BZY with increasing temperature, which is consistent with the findings of previous studies [20,32]. Figure 8b illustrates the current–voltage behavior of the electrolyte-supported cell (Pt/BZY/Pt). The power density of the fuel cell increases with increasing temperature. The maximum powder density value obtained in this study was 5.24 $mW \cdot cm^{-2}$ at 900 °C, which is comparable to the values reported in the literature for electrolyte-supported cells produced using Y-doped $BaZrO_3$-based electrolytes (1–1.2 mm thick) and ZnO and CuO sintering aids [14,16].

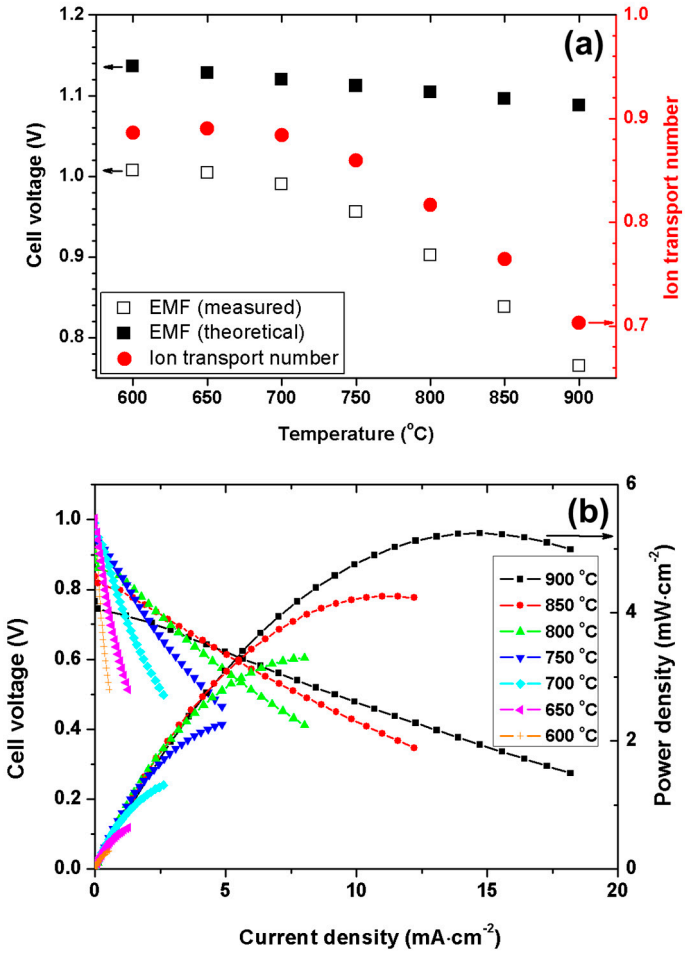

Figure 8. (**a**) EMF values measured for the Pt/BZY/Pt cell, together with the theoretical electromotive force (EMF) and total ion transport number, and (**b**) current–voltage and power density curves of the BZY-supported cell with Pt/BZY/Pt configuration for an electrolyte thickness of 1 mm.

4. Conclusions

Dense $BaZr_{0.8}Y_{0.2}O_{3-\delta}$ proton-conducting ceramics were successfully prepared by solid-state reactive sintering at different sintering temperatures of 1435, 1485, and 1535 °C over a range of sintering times of 5, 10, 15, 20, and 25 h. Additional planetary ball milling conducted after ball milling increased the density of sintered $BaZr_{0.8}Y_{0.2}O_{3-\delta}$ to levels higher than 93%, because of the decreasing particle size with narrow distribution of the precursor mixture. Conventional and synchrotron X-ray diffraction data confirmed that an unreacted Y_2O_3 phase was formed in the $BaZr_{0.8}Y_{0.2}O_{3-\delta}$ samples sintered at a relatively low temperature of 1435 °C, whereas a secondary BaY_2NiO_5 phase was observed in the samples sintered at temperatures above 1485 °C. Electrochemical impedance analysis showed that the sample sintered at 1485 °C for 15 h had the highest proton conductivity. The proton conductivity and ion transport number values of $BaZr_{0.8}Y_{0.2}O_{3-\delta}$ obtained in this study were comparable to the values reported in the literature for $BaZr_{1-x}Y_xO_{3-\delta}$. The current–voltage behavior of a symmetric $BaZr_{0.8}Y_{0.2}O_{3-\delta}$-supported cell with Pt electrodes exhibited a maximum power density of 5.24 $mW{\cdot}cm^{-2}$ at 900 °C, which is also comparable to the values reported in the literature for $BaZr_{1-x}Y_xO_{3-\delta}$ electrolytes. We expect that such detailed investigation on the physical and electrochemical properties of $BaZrO_3$-based electrolytes with various sintering conditions, including sintering time and temperature, and type of milling process, offers new insights into their practical utilization in PCFCs.

Author Contributions: Conceptualization, Y.C. and C.-Y.Y.; methodology, J.K., S.-J.K., and J.-H.L.; investigation, J.-N.K., H.C.Y., J.H.Y., M.K., and H.Y.; writing original draft preparation: D.S.Y., Y.C., and C.-Y.Y.; review and editing, Y.C. and C.-Y.Y.

Funding: This work was conducted under the framework of the Research and Development Program of the Korea Institute of Energy Research (KIER) (B8-2461-02). This work was also supported by the Soonchunhyang University Research Fund. Dr. Laura Navarrete (Universidad Politécnica de Valencia, Spain) and Jong Hyun Park (Chungnam National University) are gratefully acknowledged for the EIS measurements and analysis.

Conflicts of Interest: The authors declare no conflicts of interest.

References

1. Iwahara, H. Technological challenges in the application of proton conducting ceramics. *Solid State Ion.* **1995**, *77*, 289–298. [CrossRef]
2. Bi, L.; Traversa, E. Synthesis strategies for improving the performance of doped-$BaZrO_3$ materials in solid oxide fuel cell applications. *J. Mater. Res.* **2013**, *29*, 1–15. [CrossRef]
3. Bi, L.; Boulfrad, S.; Traversa, E. Steam electrolysis by solid oxide electrolysis cells (SOECs) with proton-conducting oxides. *Chem. Soc. Rev.* **2014**, *43*, 8255–8270. [CrossRef] [PubMed]
4. Babilo, P.; Uda, T.; Haile, S.M. Processing of yttrium-doped barium zirconate for high proton conductivity. *J. Mater. Res.* **2007**, *22*, 1322–1330. [CrossRef]
5. Fabbri, E.; Pergolesi, D.; Licoccia, S.; Traversa, E. Does the increase in Y-dopant concentration improve the proton conductivity of $BaZr_{1-x}Y_xO_{3-\delta}$ fuel cell electrolytes? *Solid State Ion.* **2010**, *181*, 1043–1051. [CrossRef]
6. Babilo, P.; Haile, S.M. Enhanced Sintering of Yttrium-Doped Barium Zirconate by Addition of ZnO. *J. Am. Ceram. Soc.* **2005**, *88*, 2362–2368. [CrossRef]
7. Han, D.; Hatada, N.; Uda, T. Chemical Expansion of Yttrium-Doped Barium Zirconate and Correlation with Proton Concentration and Conductivity. *J. Am. Ceram. Soc.* **2016**, *99*, 3745–3753. [CrossRef]
8. Shirpour, M.; Rahmati, B.; Sigle, W.; van Aken, P.A.; Merkle, R.; Maier, J. Dopant Segregation and space charge effects in proton-conducting $BaZrO_3$ perovskites. *J. Phys. Chem. C* **2012**, *116*, 2453–2461. [CrossRef]
9. Shirpour, M.; Merkle, R.; Maier, J. Space charge depletion in grain boundaries of $BaZrO_3$ proton conductors. *Solid State Ion.* **2012**, *225*, 304–307. [CrossRef]
10. Sun, Z.; Fabbri, E.; Bi, L.; Traversa, E. Electrochemical Properties and Intermediate-Temperature Fuel Cell Performance of Dense Yttrium-Doped Barium Zirconate with Calcium Addition. *J. Am. Ceram. Soc.* **2012**, *95*, 627–635. [CrossRef]

11. Cervera, R.; Oyama, Y.; MIyoshi, S.; Kobayashi, K.; Yagi, T.; Yamaguchi, S. Structural study and proton transport of bulk nanograined Y-doped $BaZrO_3$ oxide protonics materials. *Solid State Ion.* **2008**, *179*, 236–242. [CrossRef]
12. Sun, Z.; Fabbri, E.; Bi, L.; Traversa, E. Lowering grain boundary resistance of $BaZr_{0.8}Y_{0.2}O_{3-\delta}$ with $LiNO_3$ sintering-aid improves proton conductivity for fuel cell operation. *Phys. Chem. Chem. Phys.* **2011**, *13*, 7692–7700. [CrossRef] [PubMed]
13. Ricote, S.; Bonanos, N.; Manerbino, A.; Sullivan, N.P.; Coors, W.G. Effects of the fabrication process on the grain-boundary resistance in $BaZr_{0.9}Y_{0.1}O_{3-\delta}$. *J. Mater. Chem. A* **2014**, *2*, 16107–16115. [CrossRef]
14. Duval, S.B.C.; Holtappels, P.; Stimming, U.; Graule, T. Effect of minor element addition on the electrical properties of $BaZr_{0.9}Y_{0.1}O_{3-\delta}$. *Solid State Ion.* **2008**, *179*, 1112–1115. [CrossRef]
15. Peng, C.; Melnik, J.; Li, J.; Luo, J.; Sanger, A.R.; Chuang, K.T. ZnO-doped $BaZr_{0.85}Y_{0.15}O_{3-\delta}$ proton-conducting electrolytes: Characterization and fabrication of thin films. *J. Power Sources* **2009**, *190*, 447–452. [CrossRef]
16. Gao, D.; Guo, R. Structural and electrochemical properties of yttrium-doped barium zirconate by addition of CuO. *J. Alloys Compd.* **2010**, *493*, 288–293. [CrossRef]
17. Tong, J.; Clark, D.; Hoban, M.; O'Hayre, R. Cost-effective solid-state reactive sintering method for high conductivity proton conducting yttrium-doped barium zirconium ceramics. *Solid State Ion.* **2010**, *181*, 496–503. [CrossRef]
18. Tong, J.; Clark, D.; Bernau, L.; Subramaniyan, A.; O'Hayre, R. Proton-conducting yttrium-doped barium cerate ceramics synthesized by a cost-effective solid-state reactive sintering method. *Solid State Ion.* **2010**, *181*, 1486–1498. [CrossRef]
19. Nikodemski, S.; Tong, J.; O'Hayre, R. Solid-state reactive sintering mechanism for proton conducting ceramics. *Solid State Ion.* **2013**, *253*, 201–210. [CrossRef]
20. Yoo, C.-Y.; Yun, D.S.; Joo, J.H.; Yu, J.H. The effects of NiO addition on the structure and transport properties of proton conducting $BaZr_{0.8}Y_{0.2}O_{3-\delta}$. *J. Alloys Compd.* **2015**, *621*, 263–267. [CrossRef]
21. Han, D.; Iihara, J.; Uemura, S.; Kazumi, K.; Hiraiwa, C.; Majima, M.; Uda, T. A high temperature reduction cleaning (HTRC) process: A novel method for conductivity recovery of yttrium-doped barium zirconate electrolytes. *J. Mater. Chem. A* **2016**, *4*, 10601–10608. [CrossRef]
22. Polfus, J.M.; Fontaine, M.-L.; Thøgersen, A.; Riktor, M.; Norby, T.; Bredesen, R. Solubility of transition metal interstitials in proton conducting $BaZrO_3$ and similar perovskite oxides. *J. Mater. Chem. A* **2016**, *4*, 8105–8112. [CrossRef]
23. Nasani, N.; Pukazhselvan, D.; Kovalevsky, A.V.; Shaula, A.L.; Fagg, D.P. Conductivity recovery by redox cycling of yttrium doped barium zirconate proton conductors and exsolution of Ni-based sintering additives. *J. Power Sources* **2017**, *339*, 93–102. [CrossRef]
24. Ciria, D.; Ben Hassine, M.; Jiménez-Melendo, M.; Iakovleva, A.; Haghi-Ashtiani, P.; Aubin, V.; Dezanneau, G. Mechanical degradation under hydrogen of yttrium doped barium zirconate electrolyte material prepared with NiO additive. *J. Power Sources* **2016**, *321*, 226–232. [CrossRef]
25. Rodríguez-Carvajal, J. Recent advances in magnetic structure determination by neutron powder diffraction. *Phys. B Condens. Matter* **1993**, *192*, 55–69. [CrossRef]
26. Fang, S.; Wang, S.; Brinkman, K.S.; Chen, F. A sinteractive Ni–$BaZr_{0.8}Y_{0.2}O_{3-\delta}$ composite membrane for hydrogen separation. *J. Mater. Chem. A* **2014**, *2*, 5825–5833. [CrossRef]
27. Yamazaki, Y.; Hernandez-Sanchez, R.; Haile, S.M. Cation non-stoichiometry in yttrium-doped barium zirconate: Phase behavior, microstructure, and proton conductivity. *J. Mater. Chem.* **2010**, *20*, 8158–8166. [CrossRef]
28. Azad, A.K.; Savaniu, C.; Tao, S.; Duval, S.; Holtappels, P.; Ibberson, R.M.; Irvine, J.T.S. Structural origins of the differing grain conductivity values in $BaZr_{0.9}Y_{0.1}O_{2.95}$ and indication of novel approach to counter defect association. *J. Mater. Chem.* **2008**, *18*, 3414–3418. [CrossRef]
29. Nomura, K.; Kageyama, H. Transport properties of $BaZr_{0.8}Y_{0.2}O_{3-\delta}$ perovskite. *Solid State Ion.* **2007**, *178*, 661–665. [CrossRef]
30. Nikodemski, S.; Tong, J.; Duan, C.; O'Hayre, R. Ionic transport modification in proton conducting $BaCe_{0.6}Zr_{0.3}Y_{0.1}O_{3-\delta}$ with transition metal oxide dopants. *Solid State Ion.* **2016**, *294*, 37–42. [CrossRef]
31. Yamazaki, Y.; Hernandez-Sanchez, R.; Haile, S.M. High Total Proton Conductivity in Large-Grained Yttrium-Doped Barium Zirconate. *Chem. Mater.* **2009**, *21*, 2755–2762. [CrossRef]

32. Tong, J.; Clark, D.; Bernau, L.; Sanders, M.; O'Hayre, R. Solid-state reactive sintering mechanism for large-grained yttrium-doped barium zirconate proton conducting ceramics. *J. Mater. Chem.* **2010**, *20*, 6333–6341. [CrossRef]
33. Kjølseth, C.; Fjeld, H.; Prytz, Ø.; Dahl, P.I.; Estournès, C.; Haugsrud, R. Space–charge theory applied to the grain boundary impedance of proton conducting $BaZr_{0.9}Y_{0.1}O_{3-\delta}$. *Solid State Ion.* **2010**, *181*, 268–275. [CrossRef]
34. Iguchi, F.; Sata, N.; Yugami, H. Proton transport properties at the grain boundary of barium zirconate based proton conductors for intermediate temperature operating SOFC. *J. Mater. Chem.* **2010**, *20*, 6265–6270. [CrossRef]